

Investigation of Induction Heating in Asphalt Mortar: Numerical Approach

Apostolidis, Panos; Liu, X.; Scarpas, Athanasios; van de Ven, Martin; van Bochove, G

Publication date

2016

Document Version

Accepted author manuscript

Published in

Investigation of Induction Heating in Asphalt Mortar: Numerical Approach

Citation (APA)

Apostolidis, P., Liu, X., Scarpas, A., van de Ven, M., & van Bochove, G. (2016). Investigation of Induction Heating in Asphalt Mortar: Numerical Approach. In *Investigation of Induction Heating in Asphalt Mortar: Numerical Approach*

Important note

To cite this publication, please use the final published version (if applicable). Please check the document version above.

Copyright

Other than for strictly personal use, it is not permitted to download, forward or distribute the text or part of it, without the consent of the author(s) and/or copyright holder(s), unless the work is under an open content license such as Creative Commons.

Takedown policy

Please contact us and provide details if you believe this document breaches copyrights. We will remove access to the work immediately and investigate your claim.

Investigation of Induction Heating in Asphalt Mortar: Numerical Approach

P. Apostolidis¹, X. Liu¹, T. Scarpas¹, M.F.C. van de Ven¹ and G. van Bochove²

¹ Section of Pavement Engineering

Faculty of Civil Engineering and Geosciences, Delft University of Technology

Stevinweg 1, 2628 CN Delft, the Netherlands

Tel. +31 61 6599128, Email: p.apostolidis@tudelft.nl

² Heijmans, Heijmans Integrale Projecten B.V.

Graafsebaan 3, 5248 JR Rosmalen, the Netherlands

Tel. +31 73 5435425, Email: gbochove@heijmans.nl

Corresponding author:

P. Apostolidis

E-mail: p.apostolidis@tudelft.nl

Total Number of Words

Words in abstract	=	141	words
Words in text:	=	4085	words
Words in references	=	517	words
Figures: (11x250)	=	2750	words equivalent
<hr/> Total	=	<hr/> 7493	<hr/> words equivalent

*Submitted for publication and presentation for the 95nd meeting of the Transportation Research Board,
January 10-14, 2016*

ABSTRACT

The research reported in this paper focuses on utilization of advanced finite-element analyses (COMSOL) for the design and assessment of the induction heating capacity of asphalt mortar by adding electrically conductive additives (e.g., steel fibers), and to understand the factors that influence the mechanisms of induction heating in asphalt mixtures. In order to determine numerically the effective electrical and thermal properties of the conductive asphalt mortar with different volumes of steel fibers, 3D finite element meshes were generated by using X-ray images and utilized for calibration of the model parameters to perform a more realistic simulation of the asphalt mixture induction heating. The findings of this research are part of a study to provide an optimization method for the development of the necessary tools and equipment that will enable the implementation of induction technology for healing of asphalt concrete mixtures.

1 INTRODUCTION

2
3 Asphalt mixtures are widely used in the construction industry mainly for the transportation infrastructure and
4 are considered to be self healing materials. Because of its natural ability to recover mechanical properties,
5 such as strength and stiffness, asphalt mixes autonomously heal during hot summers and long rest periods (1-
6 4). This self healing capacity of asphalt mixes has a large impact on the service life of the asphalt pavements.
7 If a fast healing process can be initiated at the right time, the lifetime of the asphalt concrete mixtures can
8 significantly be prolonged. In this case the life cycle cost can be reduced and also the traffic disruptions due
9 to maintenance activities can be minimized.

10 Induction heating techniques have been applied widely in the metallurgical and semiconductor industry
11 for bonding, hardening or softening of metals or conductive materials (5-7). Recently, efforts were made to
12 develop innovative techniques to accelerate the healing capability of asphalt mixes, see Figure 1, (8-12). It
13 has been shown that the induction heating of asphalt mixtures can significantly improve the mechanical
14 performance of asphalt mixes by healing of the micro-cracks and preventing the formation of macro-cracks.

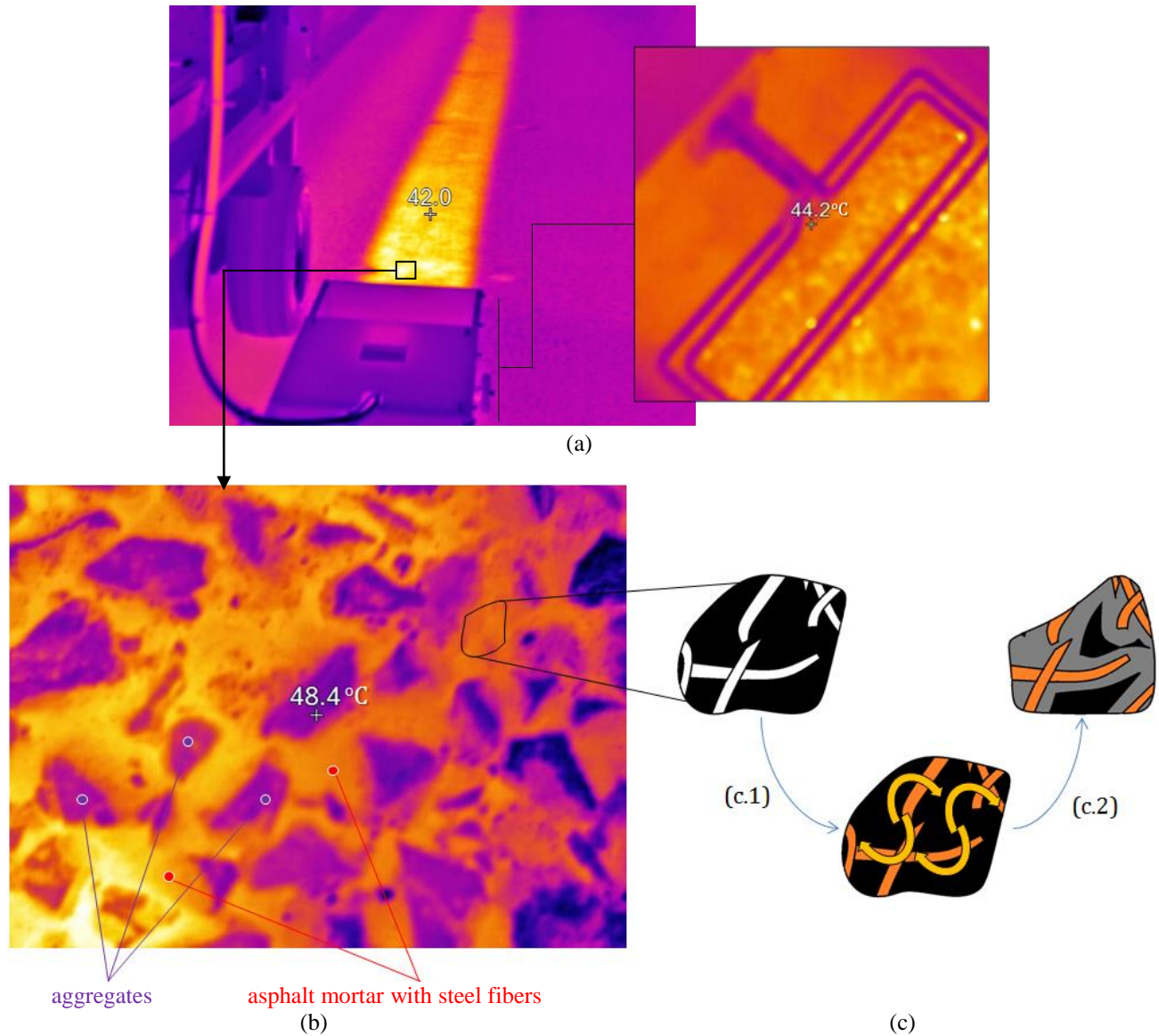
15 However, more data is still required to clarify the role and the significance of the various parameters on
16 the asphalt heating phenomenon. Particularly, induction heating is a complex phenomenon that combines the
17 electromagnetic and heat transfer theory, and has a strong relationship with the electro-magneto-thermal
18 properties of materials (13-15). The necessity of experimental and numerical analysis of electro-magneto-
19 thermo-mechanical properties of asphalt mixtures is becoming very important in terms to determine the most
20 crucial material parameters for obtaining enhanced durability, simultaneously with high induction heating
21 rate.

22 It is well known that asphalt concrete mixtures are characterized as non-conductive materials, but when
23 conductive additives are mixed into the asphalt mixtures, they become suitable for induction heating. The
24 asphalt mixtures can be heated locally under a time-variable magnetic. Specifically, when an alternating
25 electric current is applied to an induction coil, a time-variable magnetic field is generated on this. According
26 to Faraday's law, this magnetic field induces currents (eddy currents) in the additives within the mixture, such
27 as steel fibers, and they are heated up based on the principles of the Joule law, see Figure 1.c. The generated
28 heat in the additives increases locally the temperature of the asphalt mortar rather than heating the stone
29 aggregates, through the temperature rise the bitumen is melting, the micro-cracks are healed and the
30 mechanical properties are recovered. This mechanism is known as induction healing of asphalt mixtures.

31 As previously described, additives are required into the asphalt mixtures in order to make them suitable
32 for induction heating. Addition of electrically conductive fibers is much more effective than to add
33 conductive filler-sized particles (9) and also the volume of these and bitumen influences the induction heating
34 efficiency (11). It was also observed that the thermal and the electrical conductivity as well as the induction
35 heating efficiency are dependent of the volume of steel fibers in asphalt mixtures (12). Consequently, apart
36 from the operational conditions – frequency, intensity of the magnetic field, etc - the efficiency of this type of
37 electromagnetic heating is dependent on the effective properties of the asphalt mixtures with steel fibers and
38 other additives.

39 It is obvious that although there has been conducted experimental studies in order to evaluate the impact
40 of conductive additives on induction heating efficiency, still limited research was issued to quantify the
41 influence of different operational parameters of an induction system on heating efficiency of asphalt mixes.
42 The present paper, which studies the important factors of induction heating in asphalt mixes, presents the
43 theoretical background of phenomena behind the induction heating technique. Asphalt mortar - asphalt mix
44 without the stone fraction - is selected to be studied here because it is the part of asphalt concrete where
45 conductive fibers are dispersed notably, contributing to the final mechanical performance and electro-thermal
46 properties of asphalt (16, 17). The 3D finite element meshes of asphalt mortars with different volumes of
47 steel fibers are generated using X-ray scans in order to evaluate the effective electrical and thermal properties.

48 After the numerical determination of important induction parameters for the conductive asphalt mortar, a
 49 finite element 3D model of electromagnetic phenomena coupled with heat transfer physics is developed. The
 50 current FE model provides us this efficient tool to conduct analysis of induction heating predicting in parallel
 51 the heating time needed in order to heal micro-cracks inside of asphalt mixes. It should be taken into account
 52 that the recommended surface temperature of asphalt mortar to obtain sufficient healing recovery is 85 °C
 53 (11).
 54



55 **FIGURE 1** Infrared image (a) during induction heating of an asphalt pavement (A58 near Vlissingen,
 56 the Netherlands), (b) of heated asphalt pavement surface at high resolution and (c) the schematic of
 57 induction heating of asphalt mortar with steel fibers (c.1) induced by eddy currents and (c.2) heat
 58 generation in the mortar based on the Joule's law

59
60
61
62
63
64
65
66
67

THEORETICAL BACKGROUND

Fundamentals of Electromagnetic Field Phenomena

Maxwell's equations describe the electromagnetic field phenomena by involving four different field variables: the electric flux density vector \mathbf{D} [C/m²] or [As/m²], the magnetic flux density vector \mathbf{B} [A/m], the electric field intensity vector \mathbf{E} [V/m] and the magnetic field intensity vector \mathbf{H} [A/m²], and are given in the following equations 1, 2, 3 and 4:

$$\nabla \times \mathbf{E} = -\frac{\partial \mathbf{B}}{\partial t} \quad (1)$$

68
69 which is known as Faraday's law and describes that the induced currents in the asphalt mixture with
70 conductive additives have the same frequency, but the opposite direction as the supplied electric current by
71 the induction coil.
72

$$\nabla \times \mathbf{H} = \mathbf{J} + \frac{\partial \mathbf{D}}{\partial t} \quad (2)$$

73
74 which is known as Ampere's law in which \mathbf{J} is the current density. The equation (2) describes that the applied
75 alternating electric current on induction coil will produce in its surrounding area an alternating magnetic field
76 with the same frequency as the induction coil current.
77

$$\nabla \cdot \mathbf{D} = \rho \quad (3)$$

78
79 which is known as Gauss's electric field law and ρ is the free volume charge density [C/m³] or [As/m³].
80

$$\nabla \cdot \mathbf{B} = 0 \quad (4)$$

81
82 which is known as Gauss's magnetic field law.
83 To include the main constitutive equations of electromagnetic phenomena, the following demonstrates the
84 relationship between the electric flux and the intensity of the field
85

$$\mathbf{D} = \varepsilon_0 \cdot \varepsilon_r \cdot \mathbf{E} = \varepsilon \cdot \mathbf{E} \quad (5)$$

86
87 wherein ε is the electric permittivity ([F/m] or [As/m]) of the asphalt mixture with conductive additives. The
88 permittivity is the product of the electric permittivity of vacuum ε_0 (8.854·10⁻¹² As/Vm) and the relative
89 electric permittivity (ε_r). The last one describes the ability of a material to conduct the electric field better
90 than vacuum or air and it is one for conductive materials.
91 The relation between the magnetic flux and field intensity is
92

$$\mathbf{B} = \mu_0 \cdot \mu_r \cdot \mathbf{H} = \mu \cdot \mathbf{H} \quad (6)$$

93
94 where μ is the permeability [H/m] or [Vs/A]. The permeability of vacuum is constant with a value $\mu_0=4\pi \cdot 10^{-7}$
95 Vs/Am. The relative magnetic permeability μ_r describes the ability of a material to conduct the magnetic
96 flux better than a vacuum or air and has a remarkable impact on all basic induction heating phenomena, coil
97 calculation and computation of electromagnetic field distribution.

98 Concerning the association of current density with the electric field density, the continuum form of Ohm's
99 law is expressed as

100

$$\mathbf{J} = \sigma \cdot \mathbf{E} \quad (7)$$

101

102 in which σ is the electrical conductivity [S/m] or [A/Vm].

103 The Maxwell equations represent a system of coupled first-order differential equations and they can be
104 reduced to two second-order equations. Then, the magnetic flux \mathbf{B} can be expressed by a vector potential \mathbf{A}
105 as:

106

$$\mathbf{B} = \nabla \times \mathbf{A} \quad (8)$$

107

108 wherein \mathbf{A} is the magnetic vector potential.

109 Based on the Faraday law from Maxwell's equations

110

$$\nabla \times \mathbf{E} = -\frac{\partial \mathbf{B}}{\partial t} = -\frac{\partial}{\partial t} (\nabla \times \mathbf{A}) = -\nabla \times \frac{\partial \mathbf{A}}{\partial t} \quad (9)$$

111

112 Due to the fact that

113

$$\nabla \times \left(\mathbf{E} + \frac{\partial \mathbf{A}}{\partial t} \right) = \nabla \times (\nabla \varphi) = 0 \quad (10)$$

114

115 then,

116

$$\mathbf{E} = -\frac{\partial \mathbf{A}}{\partial t} - \nabla \varphi \quad (11)$$

117

118 Multiplication of the electric field with the electrical conductivity σ gives

119

$$\mathbf{J} = \sigma \mathbf{E} = -\sigma \frac{\partial \mathbf{A}}{\partial t} - \sigma \nabla \varphi = -\sigma \frac{\partial \mathbf{A}}{\partial t} + \mathbf{J}_s \quad (12)$$

120

121 in which \mathbf{J}_s is the source current density in the induction coil.

122 Assuming that the simplification of divergence of a curl is zero and the displacement current is negligible
123 in a material with high electrical conductivity

124

$$\nabla \times \mathbf{H} = \mathbf{J} \quad (13)$$

125

126 Results in

127

$$\nabla \times \frac{1}{\mu} \mathbf{B} = \mathbf{J} \quad (14)$$

128

129 Substituting equations, the diffusion equation is

130

$$\sigma \frac{\partial \mathbf{A}}{\partial t} - \frac{1}{\mu} \nabla^2 \mathbf{A} = \mathbf{J}_s \quad (15)$$

131

132 In the case of working with the sinusoidal current excitation, and the sinusoidal eddy current as well, a
133 time-harmonic electromagnetic field is introduced

134

$$i\omega\sigma\mathbf{A} - \frac{1}{\mu} \nabla^2 \mathbf{A} = \mathbf{J}_s \quad (16)$$

135

136 In the electrically conductive asphalt mixture is an induced current density denoted by \mathbf{J}_{eddy} . The equation
137 for the asphalt mixture is

138

$$i\omega\sigma\mathbf{A} - \frac{1}{\mu} \nabla^2 \mathbf{A} = 0 \quad (17)$$

139

140 where

141

$$-i\omega\sigma\mathbf{A} = \mathbf{J}_{\text{eddy}} \quad (18)$$

142

143 **Fundamentals of Heat Transfer Phenomena**

144 Heat transfer occurs in three different modes, conduction, convection and radiation. With regards to the heat
145 conduction mode, the constitutive equation of the Fourier law is given by

146

$$q_{\text{cond}} = -k\nabla T \quad (19)$$

147

148 where k is the thermal conductivity tensor of the asphalt mixture [$\text{W}/(\text{m}^\circ\text{C})$], T is the temperature [$^\circ\text{C}$] and
149 q_{cond} is the heat flux by conduction.

150 The heat convection from the surface of the mixture to the ambient fluid or gas can be defined by the
151 following equation 20

152

$$q_{conv} = h(T_s - T_\infty)^a \quad (20)$$

153
154 where h is the convection surface heat transfer coefficient [$W/(m^2\text{C})$], T_s is the surface temperature [$^\circ\text{C}$], T_∞
155 is the ambient temperature [$^\circ\text{C}$] and q_{conv} is the heat flux density by convection [W/m^2].

156 Moreover, heat losses transferred from the hot conductive asphalt mixture due to the electromagnetic
157 radiation is known as thermal radiation and is described by equation 21

158

$$q_{rad} = \sigma \cdot em[(T_s)^4 - (T_\infty)^4] \quad (21)$$

159
160 where σ is the Stefan-Boltzmann constant ($\sigma=5.67 \cdot 10^{-8}W/m^2K^4$) and em is the emissivity of the
161 surface.

162

163 Induction Heating Coupling Equations

164 A finite element model predefined in the COMSOL Multiphysics software (19, 20), which can simulate
165 electro-magnetic and thermo-mechanical phenomena in a real time system, has been utilized for modelling of
166 the induction heating in the conductive asphalt mortar. The electromagnetic field is modeled by means of the
167 magnetic field intensity vector \mathbf{A} [A/m^2] and the magnetic flux density vector \mathbf{B} [A/m] as shown in equation
168 22

169

$$(j\omega\sigma - \omega^2\varepsilon_0\varepsilon_r)\mathbf{A} + \nabla \times \left(\frac{1}{\mu_0\mu_r} \mathbf{B} \right) - \sigma\mathbf{v} \times \mathbf{B} = J_\varphi^e \quad (22)$$

170

171 where J denotes the imaginary unit and ω the angular frequency of the harmonic current.

172 The model was created by using a Single-Turn Coil domain feature and the governing equation of the
173 induction coil under frequency-transient study analysis is given by:

174

$$I_{coil} = \int_{\partial\Omega} \mathbf{J} \cdot \mathbf{n} \quad (23)$$

175

176 where I_{coil} denotes the flowing current of the coil.

177

178 Finally, the heating equation governed by the Fourier heat transfer equation is defined by:

179

$$\rho c_p \frac{\partial T}{\partial t} + \rho c_p \mathbf{u} \cdot \nabla T = \nabla \cdot (k\nabla T) + Q \quad (24)$$

180

181 where ρ is the density, c_p is the specific heat capacity, k is the thermal conductivity and Q is the energy
182 generated in the asphalt mixture per unit volume and time.

183

183 NUMERICAL DETERMINATION OF ELECTRO-THERMAL PROPERTIES OF 184 ASPHALT MORTAR

185

186 Previous researches (9, 12) indicated that, by adding electrically conductive additives (e.g., steel fibers), an
187 asphalt mixture can be heated up in a very short time by using the induction heating technology. In order to

188 simulate the effective electrical and thermal properties of conductive asphalt mixtures, the 3D finite element
189 meshes of conductive asphalt mortars - as a representative of the asphalt mixtures without stone aggregates -
190 with different volumes of steel fibers are generated by using High-resolution X-ray CT (Computed
191 Tomography) images.

192 The High-resolution X-ray CT is a completely nondestructive technique for visualizing features in the
193 interior of opaque solid objects, and for obtaining digital information on their 3-D geometries and properties.
194 By the X-ray CT technology, the different densities of individual components (e.g., sand, filler, air voids and
195 bitumen) in the asphalt mortar can be distinguished by the gray levels in a CT slice.

196 SIMPLEWARE software was utilized to comprehensively process 3D image data and to generate volume
197 and surface meshes from the image data (18). Meshes can be directly imported into the COMSOL
198 Multiphysics finite-element software for the electrical and thermal conductivity analyses. The process of
199 reconstruction of 3D images of conductive asphalt mortars is illustrated in Figure 2.a. The 3D images of the
200 asphalt mortar with different steel fibers contents are presented in Figure 2.b.

201 For the determination of electro-thermal properties of the conductive asphalt mortar, it is necessary to
202 predefine the properties of individual components in the asphalt mortar. Therefore, in this investigation, the
203 magnitudes of the electrical and thermal conductivity of the bitumen, mineral filler and sand were assumed to
204 be $9e-5$ S/m and 0.487 W/(m·K) respectively and for steel fiber $20e+3$ S/m and 16 W/(m·k) were assumed.
205 The effective electrical and thermal conductivities of the conductive asphalt mortar with different volume
206 fractions of fiber are determined numerically and given in Figure 3.

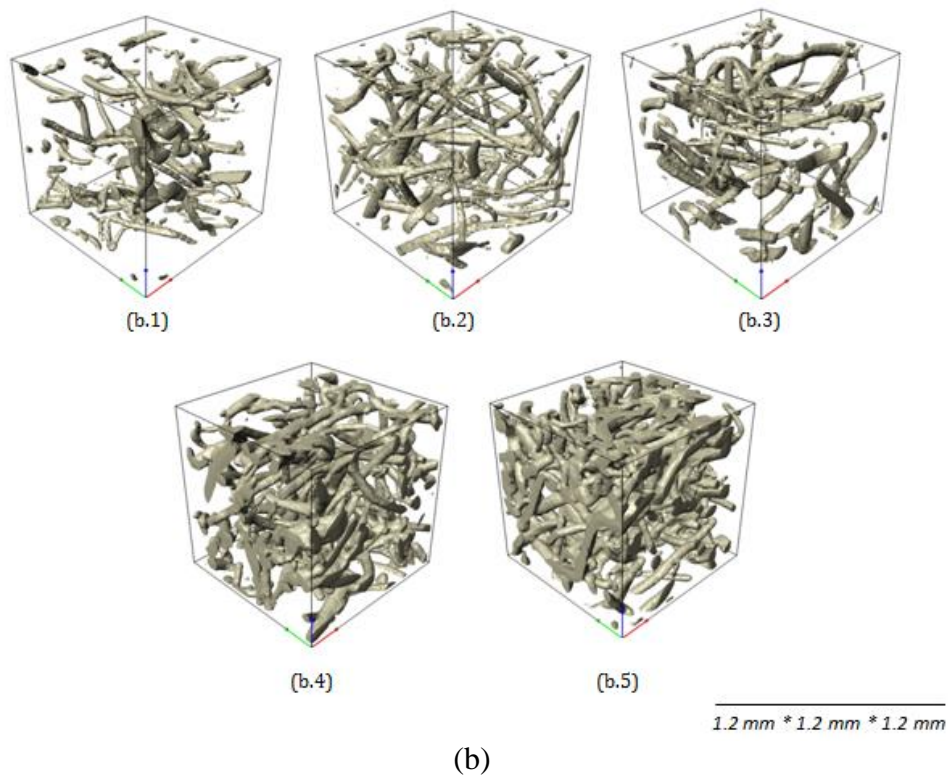
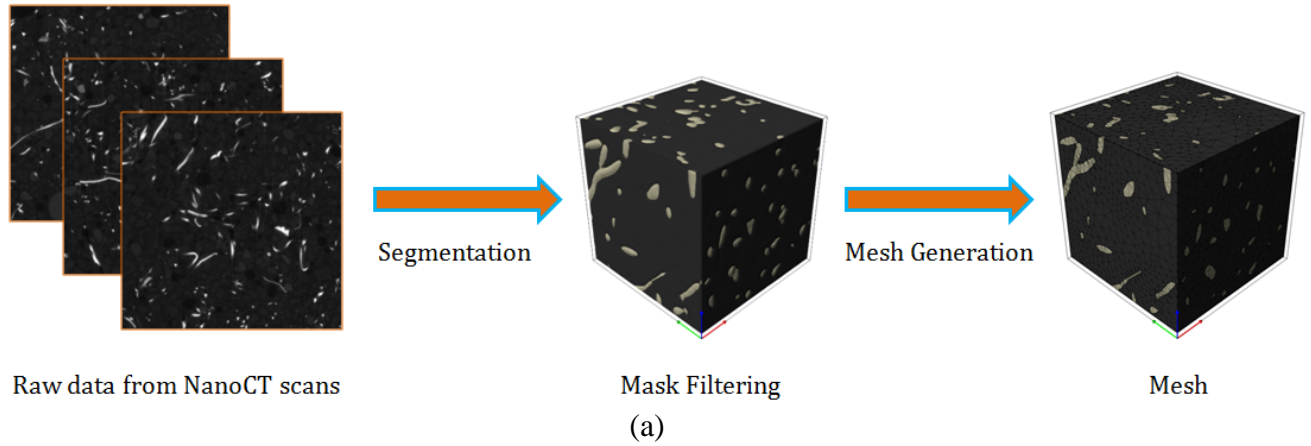
207 The results in Figure 3 indicate that the electrical conductivity of the asphalt mortar increased with
208 increasing the content of steel fiber. As it can be noticed, the electrical conductivity of the asphalt mortar
209 increases rapidly when the volume fraction of the steel fiber is close to 6%. The reason of this dramatic
210 increase of the electrical conductivity can be explained by the percolation threshold theory. The percolation
211 threshold is reached when the shorter conductive pathways are formed by the higher amount of steel fibers in
212 the asphalt mortar. Similarly, it can be observed that, with the stepwise increase of steel fibers in the asphalt
213 mortar, the effective thermal conductivity of the conductive asphalt mortar is increased from 0.71 W/(m·K) to
214 1.58 W/(m·K). This happened because the thermal conductivity of steel fibers is higher than the other
215 components in the asphalt mortar.

216 According to the current numerical analysis, the improvement of effective electrical and thermal
217 conductivity is dependent on the proportion of steel fibers in the asphalt mortar. Moreover, it is well known
218 that it is difficult to obtain experimentally precise conductivity results from asphalt mixtures (16). Therefore,
219 this method of numerical analysis of asphalt mortar properties could be proved effective tool to determine the
220 electro-thermal characteristics of conductive asphalt mixes. Subsequently, understanding the conductivity
221 mechanism is also the other advantage of this numerical technique where the transformation phenomenon of
222 asphalt mix, from insulator to conductor, can be quantified by identifying the percolation threshold limit.

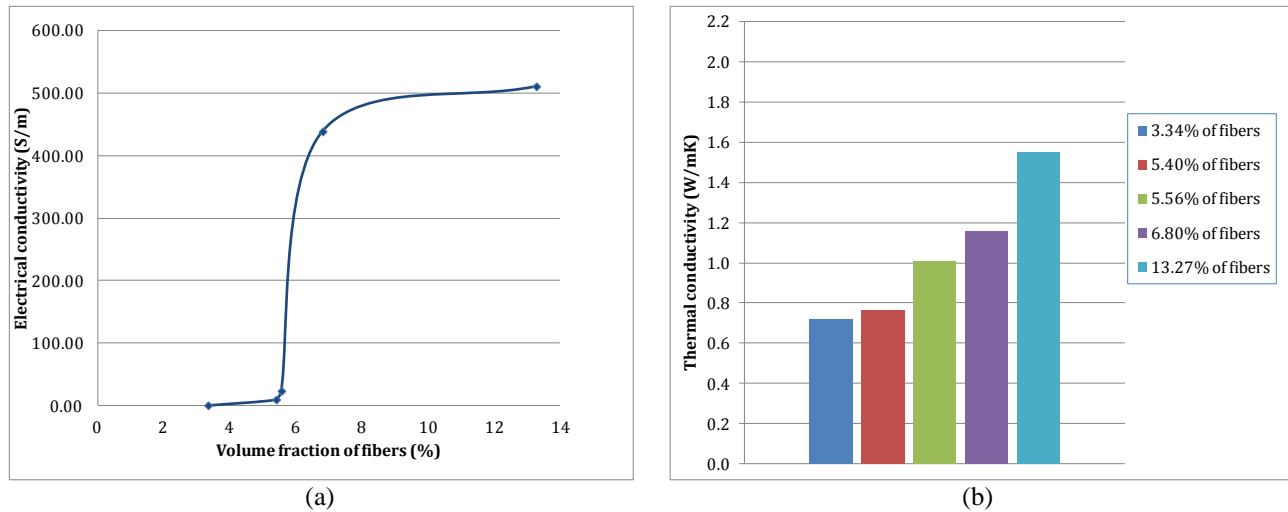
223

224

225



226
 227 **FIGURE 2 (a) Overview of 3D image data post processing and (b) reconstructed images after**
 228 **segmenting the NanoCT-scans for the conductive asphalt mortars with different steel fibers content;**
 229 **(b.1) 3.4 %, (b.2) 4.7 %, (b.3) 5.2 %, (b.4) 6.8 % and (b.5) 13.3 % of steel fibers**
 230



231 **FIGURE 3 Numerically determined effective (a) electrical and (b) thermal conductivity of different**
 232 **asphalt mortars**

233

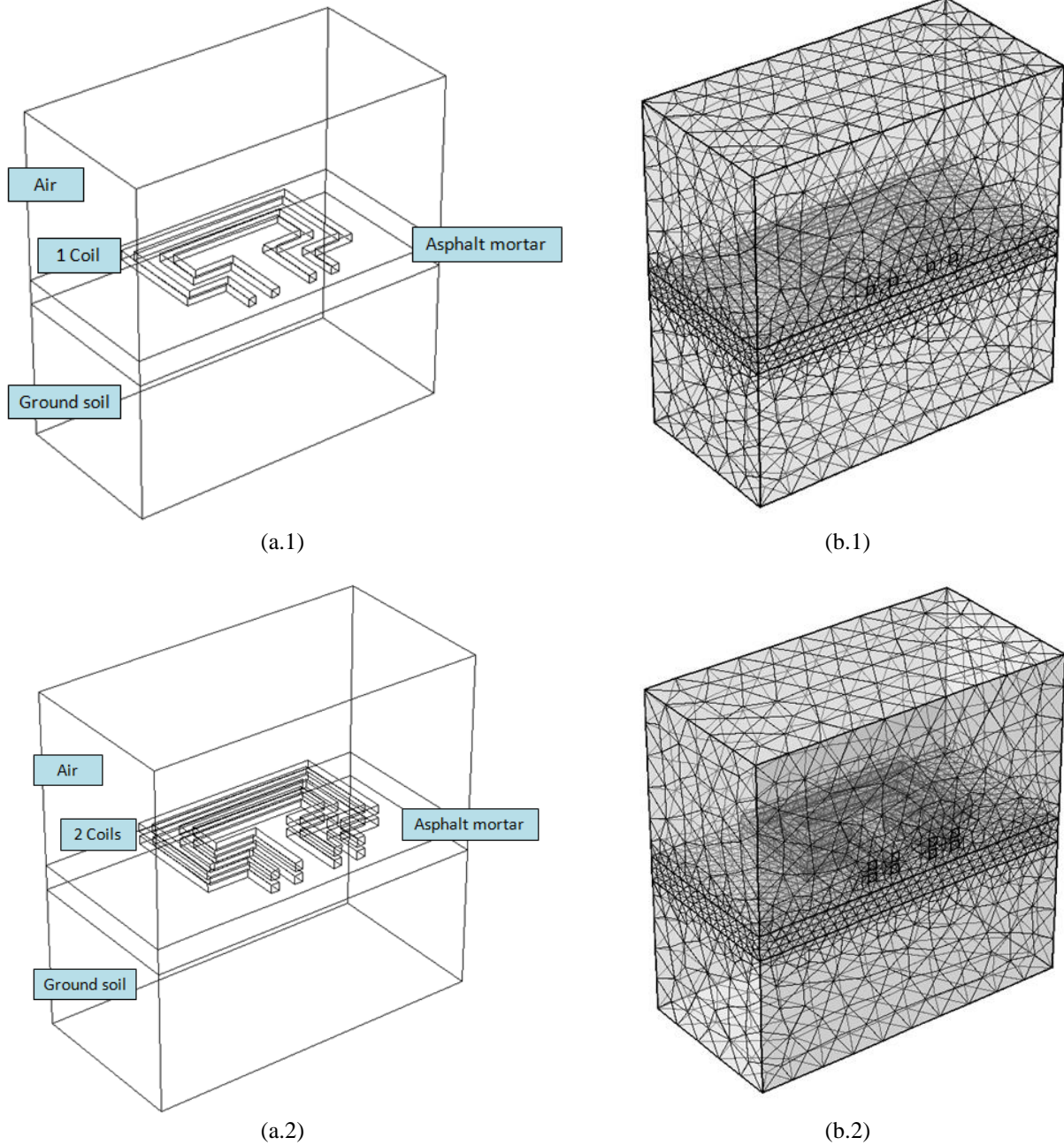
234 FINITE ELEMENT MODELS AND PARAMETERS

235

236 In order to study the influence of frequency, power and distance of coils on the induction heating capacity of
 237 the conductive asphalt mortar, two finite element (FE) models were utilized. One model makes use of one
 238 induction coil at a distance of 50 mm above the surface of the mortar sample, Figure 4.a.1. In the second
 239 model, an additional coil is used at a distance of 200 mm above the surface of the mortar, Figure 4.a.2. The
 240 induction coils with a square cross-section of side 0.1 m were assumed. By imposing the alternative current to
 241 the coils, eddy current can be generated in the vicinity of the conductive asphalt mortar. It should be noted
 242 that the geometry of the induction coil has significant impact on the induction heating efficiency (5, 6). For
 243 this reason, the higher order tetrahedral elements were utilized to model the coils and the entire induction
 244 heating system, see Figure 4.b.1 & b.2. In addition to the coils, each model consists of one layer of the
 245 conductive asphalt mortar with a thickness of 30 cm, one layer of ground sand soil underneath the mortar
 246 layer and air above the mortar layer.

247 Normally the electrical-thermal properties of conductive asphalt mixtures are temperature dependent.
 248 However, for simplicity, the electro-thermal properties of the conductive asphalt mortar are assumed constant
 249 in the simulations.

250 In order to make the asphalt mortar conductive, it was assumed that 6% of steel fibers was added into the
 251 asphalt mixture. The electrical and thermal conductivity of the conductive asphalt mortar were taken from the
 252 numerical analysis from the previous section. Furthermore, in the following numerical simulations, the
 253 parameters of the relative permeability and heat capacity of the conductive mortar were assumed to be 1 and
 254 920 J/(kg·K) respectively. Moreover, an ambient temperature of 20 °C was assumed to simulate the induction
 255 heating operation at normal environmental conditions. The duration of the induction heating in the simulation
 256 was 120 second. The applied power voltage and the frequency of the alternating magnetic field were set to
 257 550 V and 64 kHz for the simulations based on previous experimental experience (12).
 258



259 **FIGURE 4 Schematic of (a.1) one coil and (a.2) two coils induction systems at 3D; and the relative**
 260 **mesh refinements (b.1 and b.2)**

261

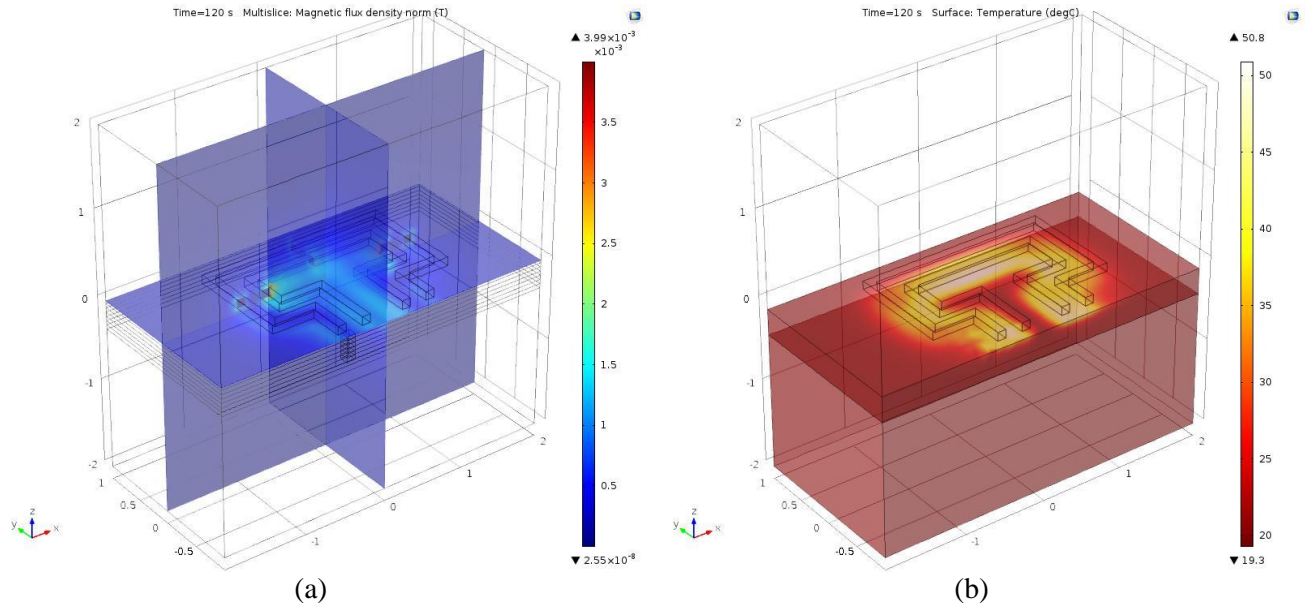
262 **RESULTS AND DISCUSSION**

263

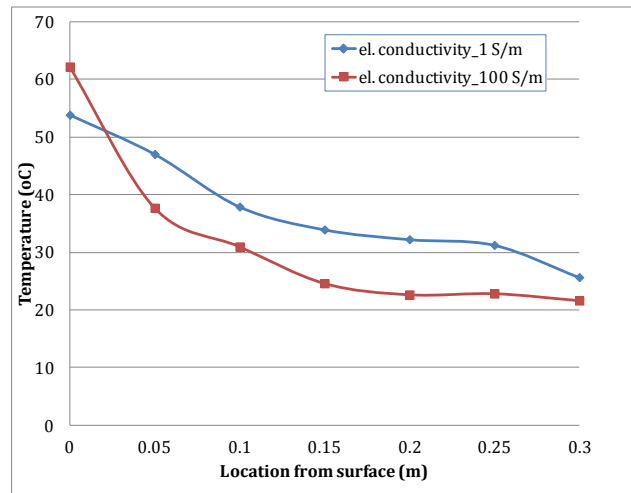
264 **Effect of Electrical and Thermal Properties**

265 The numerical simulations for the one coil system were carried out first. The distribution of magnetic flux
 266 density and temperature on the conductive asphalt mortar are shown in Figure 5. The influence of the

267 electrical conductivity on the temperature distribution within the cross-section of the asphalt mortars is shown
 268 in Figure 6. It should be noted that the asphalt mortar with 100 S/m of electrical conductivity corresponds to
 269 the response of the asphalt mortar mixed with 6% of steel fibers. Hence, the asphalt mortar with 1 S/m of
 270 electrical conductivity represents the mortar mixed with a very low amount of steel fibers.
 271



272 **FIGURE 5 (a) Magnetic flux density and (b) temperature distribution at the end of induction heating**
 273



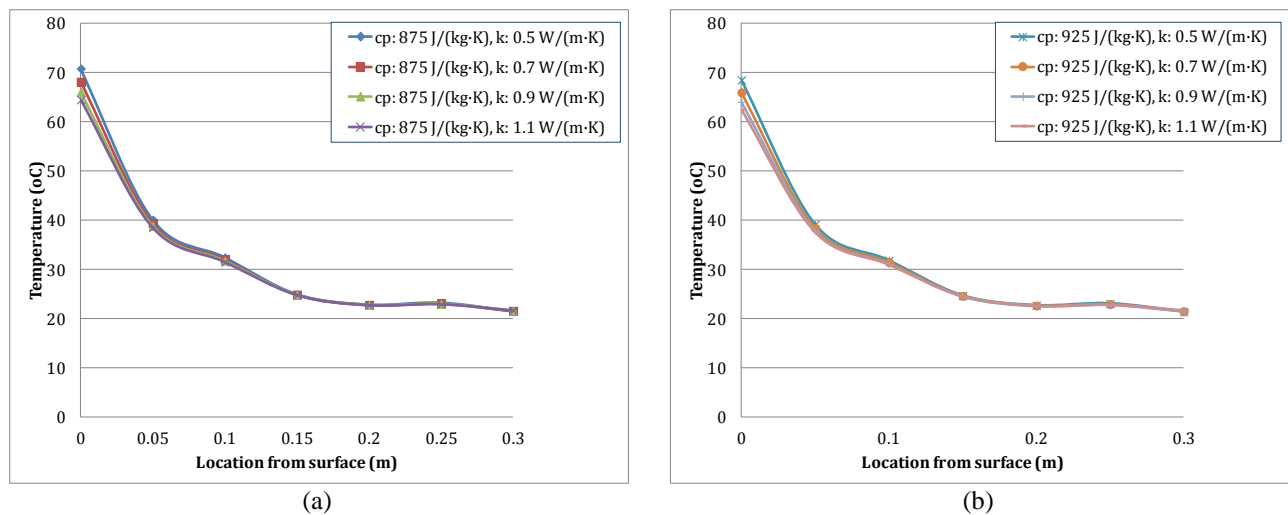
274 **FIGURE 6 Influence of the electrical conductivity of the conductive asphalt mortars on temperature**
 275 **distribution (induction time 120s, one induction coil system)**
 276
 277
 278

279 It can be observed in Figure 6 that, after 120 seconds of induction heating, for the case of the asphalt
 280 mortar with 100 S/m of electrical conductivity, the surface temperature is higher than with 1 S/m (lower
 281 amount of steel fibers). This finding supports the observations made by previous researches (12), where the

282 induction heating efficiency appears to be proportional to the volume of the conductive additives added in the
 283 asphalt mixes.

284 The amount of steel fibers can also influence the thermal gradient inside the asphalt mortar, see Figure 6.
 285 For example, for the case of asphalt mortar with 100 S/m of electrical conductivity, the temperature decreases
 286 faster inside the mortar, than the case 1 S/m. This thermal gradient difference is caused by the skin effect.
 287 When a conductive asphalt mortar has a high electrical conductivity, the alternating magnetic field induces
 288 electric currents which are concentrated on the surface of the conductive asphalt mortar. The high
 289 concentration of the electric currents leads to a higher heat generation at the surface of the conductive asphalt
 290 mortar. Therefore the asphalt mortar with higher electrical conductivity (e.g., 100 S/m) has a higher
 291 temperature at the surface but a lower temperature inside the material.

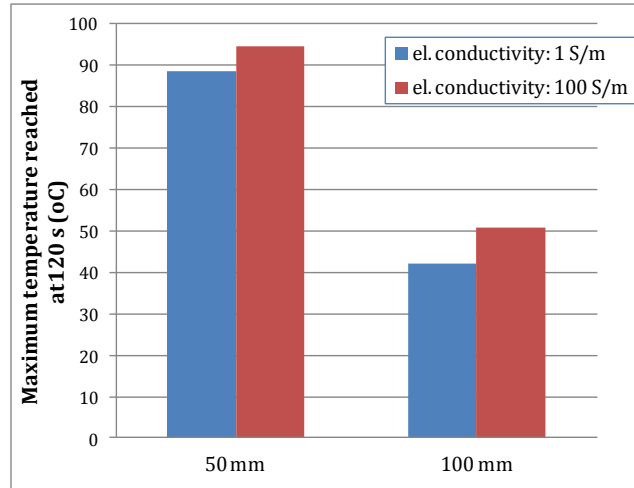
292 In Figure 7, the effect of thermal conductivity and heat capacity of conductive asphalt mortars is also
 293 presented. The parametric analyses are done for conductive asphalt mortar with two different heat capacities
 294 (e.g., 875 and 925 J/(kg·K)), four different thermal conductivities(e.g., 0.5, 0.7, 0.9, 1.1 W/(m·K)), while the
 295 electrical conductivity of the compared mortars is constant (100 S/m). By comparing to Figure 6, it can be
 296 concluded that the impact of the thermal properties of the asphalt mortar on the temperature distribution is not
 297 of the same importance with the effect of electrical conductivity.
 298



299 **FIGURE 7 Influence of the thermal conductivity and heat capacity of the conductive asphalt mortars**
 300 **on temperature distribution (electrical conductivity 100 S/m, induction time 120s, one induction coil**
 301 **system)**

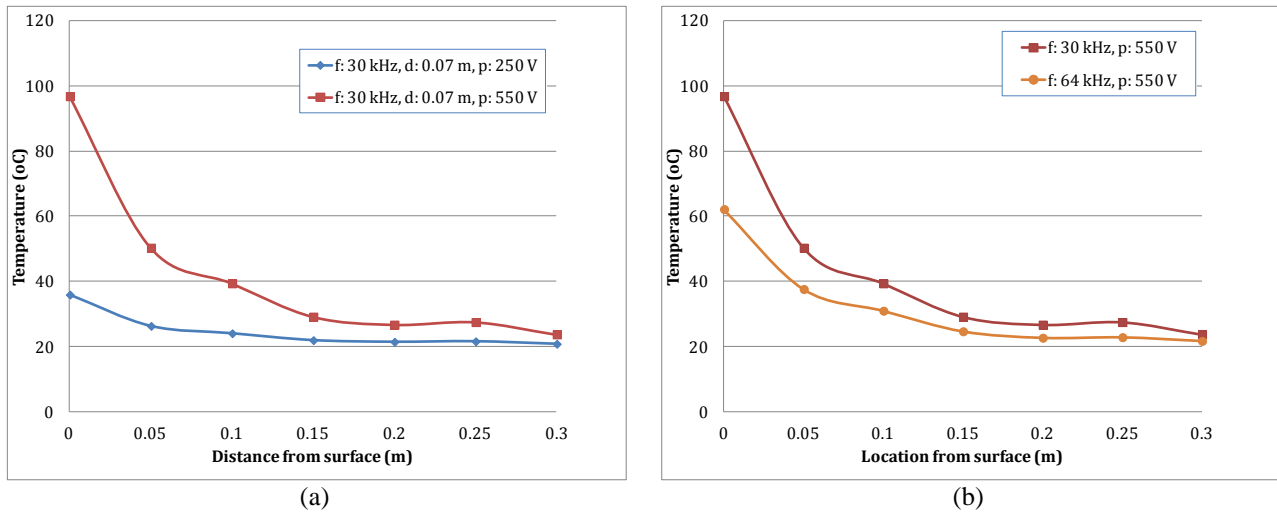
303 Effect of Operational Parameters

304 The numerical results in Figure 8 show that the distance between the induction coil and the conductive mortar
 305 can influence significantly the heat generation in the conductive asphalt mortar. By increasing the coil
 306 distance from 50 mm to 100 mm to the mortar surface, it leads to 50% reduction of the temperature at the
 307 surface of the asphalt mortar. This means that for surface induction heating coil closer to the surface is more
 308 efficient one at larger distance from the surface of the asphalt mortar. Moreover, the tendency is similar for
 309 the materials with different electrical conductivity values.
 310



311
 312 **FIGURE 8** Maximum temperature generated by the single coil system at the different electrical
 313 conductivities at the different coil distances to the conductive asphalt mortar (one induction coil
 314 system)
 315

316 The power and the frequency of the alternating magnetic field of the induction machine are two important
 317 operational parameters that can influence significantly the induction heating efficiency of the conductive
 318 asphalt mortar. Figure 9 shows the comparison of the effect of the power and the frequency of the induction
 319 coil on the temperature distribution inside the conductive asphalt mortar. It can be observed that, at the same
 320 frequency (e.g., 30 kHz), higher machine power results in higher temperatures generated in the material over
 321 the whole height.
 322



323 **FIGURE 9** Influence of (a) the supplied power and (b) the frequency of induction coil (electrical
 324 conductivity 100 S/m, induction time 120s, one induction coil system)
 325

326 On the other hand, the frequency of the magnetic field is another important operation parameter. It can be
 327 seen that, at constant voltage (e.g., 550 V), the lower frequency of 30 kHz leads to higher maximum surface

328 temperature than the higher frequency of 64 kHz. The distributions of the temperature within the cross-
 329 section of the conductive asphalt mortar show the same tendency for the both cases.

330

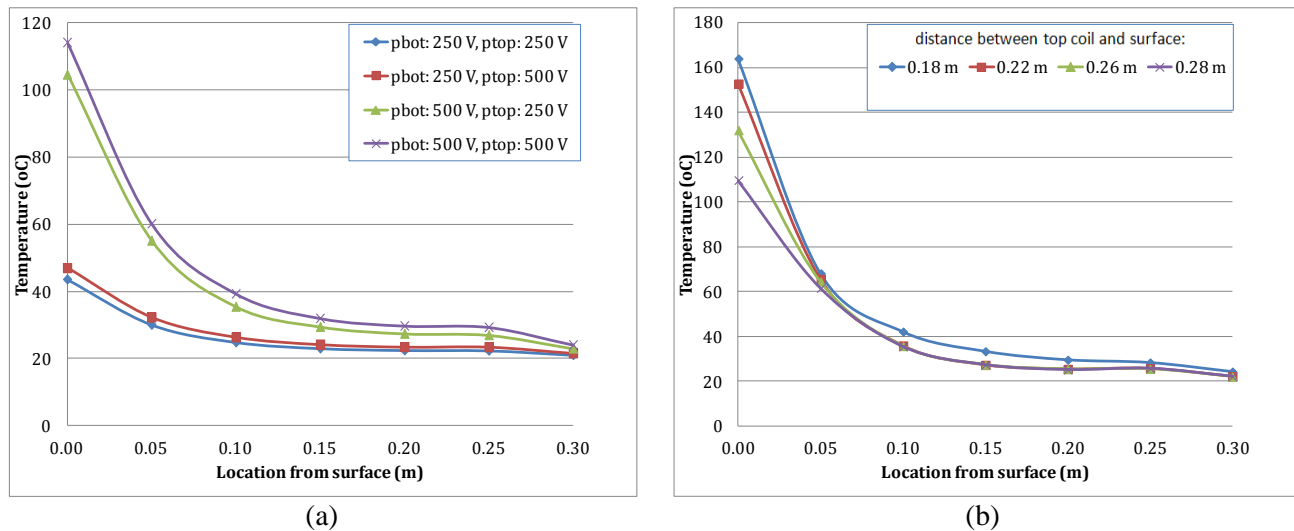
331 **Effect of Two Coils Induction System**

332 In order to show the possibilities for guidance for the induction machine design, the influence of two coils
 333 system on the heating efficiency of the asphalt mortar was also studied. The influence of the supplied powers
 334 of the two induction coils system and the distance of the upper induction coil to the sample surface is
 335 presented.

336 Figure 10.a shows the plots of the temperature distribution in the asphalt mortar with 6% of steel fibers for
 337 the different combinations of the power of the bottom and the top induction coil. It can be observed that the
 338 power of the coil closer to the surface of the induction material has a significant effect on the heat generation.
 339 When the power of both coils is doubled from 250 V to 500 V, the induction heating efficiency of the system
 340 increases by 8%. The distributions of the temperature within the cross-section of the conductive asphalt
 341 mortar show the same tendency for both cases.

342 With the bottom coil at constant distance (50 mm) to the sample surface, the induction heating efficiency
 343 decreases with increasing the distance of the top coil, see Figure 10.b. Increase of the distance of the top coil
 344 to the sample surface from 180 mm to 280 mm, leads to reduction of the heat efficiency. Despite the fact that
 345 the maximum temperature drops because of the increase of the distance of the top coil to the sample surface,
 346 the distribution of the temperature within the cross-section of the conductive asphalt mortar show the same
 347 tendency for all the cases.

348



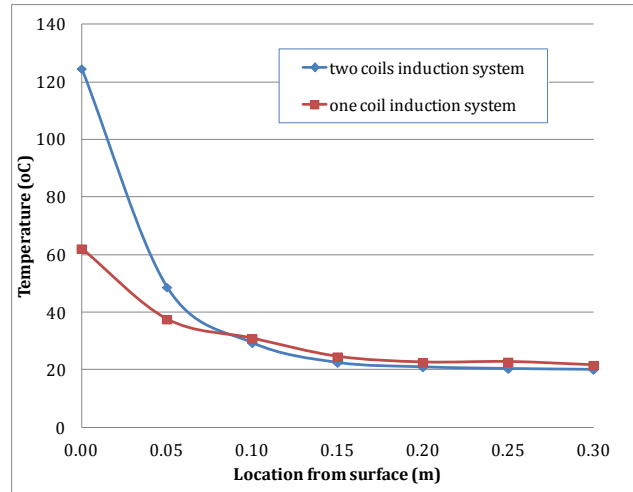
349

350 **FIGURE 10 Influence of (a) the supplied powers of the two induction coils system (frequency 64.5 kHz,**
 351 **electrical conductivity 100 S/m, induction time 120s) and (b) the distance of the upper induction coil to**
 352 **the sample surface (frequency 64 kHz, electrical conductivity 100 S/m, induction time 120s)**

353

354 Finally, a comparison of the two coils system with the one coil system is presented in Figure 11. It can be
 355 observed that, at the same induction time (120 s), the two coils induction system generates two times higher
 356 surface temperature the one coil induction system. Also, the two coil induction system is more powerful and
 357 efficient for asphalt concrete healing application, because it can generate higher temperatures in the top part
 358 of the first layer which enables the contractor to heal the micro cracks quickly at this place. Thus, the

359 induction heating technique can be approved very highly efficient for preserving pavement surface defects,
 360 such as the raveling, when two coils systems are utilized.
 361



362
 363
 364 **FIGURE 11 Comparison of the different types of induction coil systems on heating distribution in the**
 365 **conductive asphalt mortar (electrical conductivity 100 S/m, induction time 120s)**
 366

367 CONCLUSIONS

368
 369 The electrical and thermal characteristics of a conductive asphalt mortar play important role for the design
 370 and assessment of the induction heating capacity of asphalt concrete mixtures. The application of FEM to
 371 evaluate the effective properties of conductive asphalt mixes and the different operational conditions of
 372 induction heating is proved to be a very effective tool, capable to perform analysis without conducting time
 373 consuming and costly experiments. The 3D induction heating FE model enables us to calibrate the model
 374 parameters to perform more realistic heating simulations for asphalt concrete mixtures. Lastly, the valuable
 375 findings of this research show that it is possible to optimize the necessary tools and equipment needed for the
 376 implementation of the induction technology for heating and subsequently healing asphalt pavements.
 377

378 REFERENCES

- 379
 380 1. Little, D.N., A. Bhasin. Exploring mechanisms of healing in asphalt mixtures and quantifying its impact. In
 381 *Self Healing Materials: An Alternative Approach to 20 Centuries of Materials Science* (S. van de Zwaag, ed.)
 382 Springer Series in Materials Science, Vol. 100, Springer, Dordrecht, the Netherlands, 2007, pp. 205-218.
 383 2. Qiu, L. *Self healing of asphalt mixtures. towards a better understanding of the mechanism*. Ph.D.
 384 Dissertation, Delft University, 2012.
 385 3. Williams, D., D.N. Little, R.L. Lytton, Y.R. Kim, Y. Kim. *Microdamage healing in asphalt and asphalt*
 386 *concrete*. Research report 7229, A&M University, College Station, 2001.
 387 4. Kim, B., R. Roque. Evaluation of healing property of asphalt mixtures. In *Transportation Research*
 388 *Record: Journal of the Transportation Research Board, No. 1970*, Transportation Research Board of the
 389 National Academies, Washington, D.C., 2006, pp. 84-91.
 390 5. Ahmed, T.J., D. Stavrov, H.E.N. Bersee, A. Beukers. Induction welding of thermoplastic composites - an
 391 overview. *Composite Part A.: Applied Science and Manufacturing*, Vol. 37, 2006, pp. 1638-1651.

- 392 6. Rapoport, E., Y. Pleshivtseva. *Optimal control of induction heating processes*. Taylor and Francis Group,
393 2007.
- 394 7. Rudolf, R., P. Mitschang, M. Neitzel. Induction heating of continuous carbon-fibre reinforced
395 thermoplastics. *Composite: Part A*, Vol. 31, 2000, pp. 1191-1202.
- 396 8. Garcia, A., E. Schlangen, M. van de Ven. Two ways of closing cracks on asphalt concrete pavement:
397 microcapsules and induction heating. *Key Engineering Materials*, Vol. 417-418, 2010, pp 573-576.
- 398 9. Garcia, A., E. Schlangen, M. van de Ven, Q. Liu. Electrical conductivity of asphalt mortar containing
399 conductive fibers and fillers. *Construction and Building Materials*, Vol. 23, 2009. pp. 3175-3181.
- 400 10. Liu, Q., W. Yu, E. Schlangen, G. van Bochove. Unravelling porous asphalt concrete with induction
401 heating. *Construction and Building Materials*, Vol. 71, 2014, pp. 152-157.
- 402 11. Liu, G., E. Schlangen, M. van de Ven. Induction healing of porous asphalt concrete. *In Transportation*
403 *Research Record,: Journal of the Transportation Research Board, No 2305*, Transportation Research Board
404 of the National Academies, Washington, D.C., 2012, pp. 95-101.
- 405 12. Garcia. A., J. Norambuena-Contreras, M.N. Parlt. Experimental evaluation of dense asphalt concrete
406 properties for induction heating purposes. *Construction and Building Materials*, 46, 2013, pp. 48-54.
- 407 13. Mesquita, R.C., J.P.A. Bastos. 3D finite element solution of induction heating problems with efficient
408 time-stepping. *IEEE Transactions of Magnetism*, Vol. 27, No. 5, 1991, pp. 4065-4068.
- 409 14. Boadi, A., Y. Tsuchida, T. Todaka, M. Enokizono. Designing of suitable construction of high-frequency
410 induction heating coil by using finite-element method. *IEEE Transactions on Magnetism*. Vol. 41, No. 10,
411 2005, pp. 4048-4050.
- 412 15. Wang, Z., W. Huang, W. Jia, Q. Zhao, Y. Wang, W. Yan. 3D Multifields FEM computation of transverse
413 flux induction heating for moving-strips. *IEEE Transactions on Magnetism*. Vol. 35, No. 3, 1999, pp. 1642-
414 1645.
- 415 16. Wu, S., P. Pan, F. Xiao. Conductive asphalt concrete: A review on structure design, performance and
416 practical applications. *Journal of Intelligent Material Systems and Structures*. 2013.
- 417 17. Anderson, D.A., T.W. Kennedy. Development of SHRP binder specification. *Journal of the Association*
418 *of Asphalt Paving Technologists*. 62, 1993, pp. 481-507.
- 419 18. *Simpleware*. ScanIP, +ScanFE, 2011.
- 420 19. *COMSOL. AC/DC Module – User’s Guide*. Version 4.4. 2013.
- 421 20. *COMSOL. Heat Transfer Module – User’s Guide*. Version 4.4. 2013.